Dictionary learning approach for image deconvolution with variance estimation

Hang Yang,[1,*] Ming Zhu,[1] Xiaotian Wu,[1] Zhongbo Zhang,[2] and Heyan Huang[3]

[1]Changchun Institute of Optics, Fine Mechanics and Physics, Chinese Academy of Science, Changchun 130033, China

[2]School of Mathematics, Jilin University, Changchun 130012, China

[3]College of Science, Changchun University, Changchun 130022, China

*Corresponding author: yanghang09@mails.jlu.edu.cn

Received 24 April 2014; revised 16 July 2014; accepted 27 July 2014;
posted 28 July 2014 (Doc. ID 210786); published 27 August 2014

In this paper, we propose a new dictionary learning approach for image deconvolution, which effectively integrates the Fourier regularization and dictionary learning technique into the deconvolution framework. Specifically, we propose an iterative algorithm with the decoupling of the deblurring and denoising steps in the restoration process. In the deblurring step, we involve a regularized inversion of the blur in the Fourier domain. Then we remove the colored noise using a dictionary learning method in the denoising step. In the denoising step, we propose an approach to update the estimation of noise variance for dictionary learning. We will show that this approach outperforms several state-of-the-art image deconvolution methods in terms of improvement in signal-to-noise ratio and visual quality.

OCIS codes: (100.0100) Image processing; (100.1830) Deconvolution; (100.3190) Inverse problems; (100.3020) Image reconstruction-restoration.

http://dx.doi.org/10.1364/AO.53.005677

1. Introduction

Image deconvolution is a classical inverse problem existing in a wide variety of image processing fields, including physical, optical, medical [1], and astronomical applications [1,2]. For example, the camera might have moved during the time the image was captured, in which case the image is corrupted by motion blur. Another common source of blurriness is out-of-focus blur.

Mathematically, the blur process corrupting the image is a convolution with a point spread function (PSF) h. A degraded image y is given by

$$y(n_1, n_2) = (h * u_{\text{orig}})(n_1, n_2) + \gamma(n_1, n_2), \quad (1)$$

where u_{orig} and y are the original image and the observed image, respectively. γ is the noise introduced in the procedure of image acquisition, and it is generally assumed to be independent and identically distributed zero-mean additive white Gaussian noise (AWGN) with variance σ^2. $*$ denotes convolution, and $1 \le n_1 \le N$, $1 \le n_2 \le N$.

In the discrete Fourier transform (DFT) domain, Eq. (1) can be written as

$$Y(k_1, k_2) = H(k_1, k_2) \cdot U_{\text{orig}}(k_1, k_2) + \Gamma(k_1, k_2), \quad (2)$$

where Y, H, U_{orig}, and Γ are the DFTs of y, h, u_{orig}, and γ, respectively.

The inversion of the blurring process is called image deconvolution. The goal of image deconvolution is to reconstruct a true image u_{orig} from a degraded image y. It is well known that the deconvolution problem is ill-posed. Thus, to obtain a reasonable image estimation, a method of reducing the noise level needs to be utilized.

Because noise is always present in natural images, even a small amount dominates the signal in high frequencies, leading to numerous artifacts. The

1559-128X/14/255677-08$15.00/0

Wiener filter [2,3] and the constrained least squares algorithm [2] can solve this problem in the frequency domain with a fast speed. However, the visual quality of the recovered image often degrades. Total-variation-based deconvolution is a popular approach; variations of this method have also been proposed in [4] fast total variation deconvolution (FTVd), [5] total variation majorization minimization (TVMM), and [6] total variation shrinkage (TVS). These methods are well known for their edge-preserving properties and generally achieve state-of-the-art results. However, their ability to describe image textures is not satisfactory. These methods usually lead to a slightly blocky result, and some fine image textures are lost.

The most recent and effective deconvolution methods usually adopt a two-step approach [7–9]: first, a regularized inversion of the blur is performed, such as Fourier regularization, then the resulting image is processed with a cleverly engineered denoising algorithm to remove artefacts. Various denoising methods have been used for this task: for instance, a Gaussian scale mixture model (GSM) [10], a shape adaptive discrete cosine transform [11], or a block matching with three-dimensional-filtering kernel regression [12,13]. It has been shown that edge-preserving-filter-based deconvolutin algorithms can achieve good results [14,15]. A regularized deblurring method blurred/sharped dictionary learning (BSDL) using a previously learned dictionary was proposed in [16]. It employed first pairs of blurry/shape images to train the dictionary; a gradient algorithm is used for solving the corresponding optimization task. There are also many other useful algorithms and additional techniques that may be found within references [17–21].

In this paper, we propose an iterative algorithm using dictionary learning for image deconvolution to integrate a Fourier regularization technique and a dictionary learning technique into the same framework. It is a new iterative scheme different from existing image deblurring methods. The iterative process consists of two parts: debluring and denoising. The deblurring step amplifies and colors the noise corrupting the image information. In the denoising step, a dictionary-learning-based approach is used to suppress the noise and artifacts. The noise variance is an important parameter for dictionary learning; therefore we propose an approach to update the estimation of noise variance in the denoising step.

A. Paper Organization

The remainder of this paper is organized as follows. Section 2 gives a brief overview of dictionary learning. Section 3 shows how the dictionary learning is used for regularizing the deconvolution problem and how to compute the regularizer. Section 4 demonstrates the effectiveness of our approach via simulation. Section 5 provides concluding remarks.

2. Learned Sparse Representations

Like some recent algorithms for image restoration [22,23], our approach is based on the sparse decomposition of image patches. Using a dictionary matrix $D = [d_1, \ldots, d_K]$ in $R^{L\times K}$, a signal $x \in R^L$ may be represented as a linear combination of a small number of atoms from a dictionary D.

In most dictionary-learning-based image processing, L is relatively small—for instance, $L = 64$ for image patches of size 8×8 pixels—when $K = L$ and D is full rank, we have a basis representation. When $K > L$, the dictionary is said to be overcomplete.

We say that the dictionary D is well adapted to a vector x when there exists a sparse vector α in R^K such that x can be approximated by the product $D\alpha$.

Besides predefined sparsifying transforms, sparse and redundant representations of image patches based on learned dictionaries have drawn considerable attention in recent years [24–26]. The image patch set $R(u) = [R_1(u), R_2(u), \ldots, R_T(u)]$ consists of T samples, with $R_t(u) \in R^L$ denoting a vectored form of the $\sqrt{L} \times \sqrt{L}$ patch extracted from image u. The sparseland model for image patches introduced by Elad and Aharon [22] suggests that every image patch $R_t(u)$ could be represented sparsely over a learned dictionary D; that is,

$$\alpha_t^* = \arg\min_{\alpha_t} \|D\alpha_t - R_t(u)\|_2^2, \quad \text{s.t.} \|\alpha_t\|_0 \le S, \qquad t = 1, 2, \ldots, T, \tag{3}$$

where S is the required sparsity level and $\|\cdot\|_0$ denotes the l_0 quasi-norm which counts the number of nonzero coefficients of the vector.

The combination of sparse and redundant representation modeling of signals, together with a learned dictionary, has shown promise in a series of applications in image processing such as image denoising, image inpainting, and medical image reconstruction [27]. Specifically, Elad and Aharon presented a method named K-means singular value decomposition (K-SVD) [22]. It is a method to learn a dictionary of features which can then be used in regularized inverse problems. K-SVD learns the underlying features assuming a sparsity-based prior, which can then be used for denoising with the objective function as

$$\{u^*, D^*, \Gamma^*\} = \arg\min_{u,D,\Gamma} \sum_{t=1}^{T} (\|D\alpha_t - R_t(u)\|_2^2 + \|\alpha_t\|_0) + \lambda\|u - b\|_2^2, \tag{4}$$

where u is the clear image, noisy data $b = u + \gamma$, $\Gamma = [\alpha_1, \alpha_2, \ldots, \alpha_T]$ denotes the sparse coefficient matrix of image patches, and $\lambda > 0$ is the regularization parameter and is empirically chosen as $\lambda = (C/\sigma)$, where σ is the standard derivation of the noise γ and C is a positive constant. Such a method is usually implemented in a two-step alternating manner: the sparse coding stage and the dictionary D update stage.

3. Dictionary-Learning-Based Deconvolution Algorithm

In this work, we intend to recover the underlying image by iteratively deblurring and denoising via

dictionary learning. Our method relies on two steps: (1) a regularized inversion of the blur in the Fourier domain and (2) a denoising step using dictionary learning. In this section, we describe these two steps in detail.

Similar to Eq. (4), the image deblurring task can be formulated into the following minimization problem:

$$\{u^*, D^*, \Gamma^*\} = \arg\min_{u,D,\Gamma} \sum_{t=1}^{T} (\|D\alpha_t - R_t(u)\|_2^2 + \|\alpha_t\|_0) + \lambda \|h * u - y\|_2^2. \quad (5)$$

In the regularization term of Eq. (5), the convolution operator h and the sparse representation $D\alpha$ are coupled; hence we resort to the splitting technique to decouple them. The problem in Eq. (5) can be converted as follows by introducing auxiliary variables v:

$$\min_{u,v,D,\Gamma} \sum_{t=1}^{T} (\|D\alpha_t - R_t(u)\|_2^2 + \|\alpha_t\|_0) + \eta \|u - v\|_2^2 + \lambda \|h * v - y\|_2^2. \quad (6)$$

We set $r = \lambda/\eta$, and obtain a sequence of constrained subproblems as follows:

$$v^{k+1} = \arg\min_{v} \|u^k - v\|_2^2 + r\|h * v - y\|_2^2, \quad (7)$$

$$\{u^{k+1}, D^{k+1}, \Gamma^{k+1}\} = \arg\min_{u,D,\Gamma} \sum_{t=1}^{T} (\|D\alpha_t - R_t(u)\|_2^2 + \|\alpha_t\|_0) + \lambda \|u - v^{k+1}\|_2^2, \quad (8)$$

A. Direct Deconvolution

The goal of deconvolution is to make a blurry image sharper. This has the positive effect of localizing information, but it has the negative side-effect of introducing new artifacts.

Considering that Eq. (7) is a simple least squares problem, we can update v with its analytic solution. In the Fourier domain, this can be solved in a single step,

$$\mathcal{F}(v^{k+1}) = \frac{\mathcal{F}(h)^* \cdot \mathcal{F}(y) + r^k \mathcal{F}(u^k)}{|\mathcal{F}(h)|^2 + r^k}, \quad (9)$$

by using the convolution theorem for the Fourier transform, where $\mathcal{F}$ is the fast Fourier transform operator and $\mathcal{F}(\cdot)^*$ denotes the complex conjugate. The plus, multiplication, and division are all component-wise operators.

The regularization parameter r^k plays an important role in our work, and it is updated in each iteration. In practice, we find that larger r^ks often cause noisy results with ringing effects, though they substantially reduce the noise variances. We should choose a smaller r^k which obtains an edge-preserving image with more noise. Then, in the denoising step, we propose a procedure that removes the leaked noise and additional image artifacts.

For an image of $N \times N$ size and the kth step, we compute the parameters r^k using the following method:

$$r^0 = \frac{N^2\sigma^2}{\|y - E(y)\|_2^2 - N^2\sigma^2}, \quad (10)$$

$$r^{k+1} = \beta r^k, \quad (11)$$

where $E(y)$ denotes the mean of y. From this equation, one can see that the larger variance of image ($\|y - E(y)\|_2^2 - N^2\sigma^2$) would obtain a smaller r^0; it can preserve the detail information, while the smaller variance of image (a smooth image) which contains a little high-frequency information will not produce the strong ringing effects with large r^0.

Parameter r is automatically adapted in iterations starting from a small value r^0; it is multiplied by β each time. This scheme is effective to speed up convergence [4].

After direct deconvolution, the inverse Fourier transform of $\mathcal{F}(v^{k+1})$ is taken. The resulting image usually contains a special form of distortions, which are removed in the denoising step of our method.

B. Artifact Removal by Dictionary Learning

Sparsity and dictionary learning have shown promising performance in denoising, and thus we integrate them into the proposed deconvolution model.

Different from fixed basis dictionaries such as bandelets [28], contourlets [29], curvelets [30], and wavelets [31], which are usually restricted to images of a certain type, the atoms of the learned basis dictionaries can be empirically learned from image examples which will apply to any family of images. Representative learned dictionaries include adaptive learned dictionaries (K-SVDs), locally learned dictionaries [32], and learned simultaneous sparse coding [33]. These sparse coding methods can work effectively for denoising because their learned dictionaries give more adaptive image priors for Bayesian estimation than fixed basis dictionaries.

The strategy to solve Eq. (8) is to alternately update the dictionary D and coefficient matrix α, the same as that used in the K-SVD [22] and dictionary learning magnetic resonance imaging (DLMRI) [23] algorithms. Specifically, in the sparse coding step, seeking the solution of Eq. (8) with respect to a fixed dictionary D is achieved by the greedy algorithm—orthogonal matching pursuit (OMP). In the dictionary updating step, the columns of the dictionary are updated sequentially one at a time using a singular value decomposition (SVD) to minimize the approximation error.

Algorithm 1: Dictionary Learning Framework

1. Initialization: $u = v^{k+1}$, $D = D^k$, σ_{k+1}^2

2. Repeat:

- Sparse Coding Stage: Use OMP method to compute the representation coefficient α for each $R_t(u)$ by approximating the solution of

$$\forall_t \min_{\alpha_t} \|\alpha_t\|_0, \quad \text{s.t.} \|D\alpha_t - R_t(u)\|_2^2 \le C_0 \sigma_{k+1}^2. \tag{12}$$

The OMP can be used again to obtain the near-optimal (recall that OMP is an approximation algorithm, and thus a true minimization is not guaranteed) set of representation coefficient α.

- Dictionary Updating Stage: For each column $t = 1, 2, \ldots, T$ in D, update them sequentially one at a time using SVD to obtain D^{k+1}:

– Find the set of patches that uses this atom, $\omega_l = \{t | \alpha_t(l) \neq 0\}$.

– For each index $t \in \omega_l$, compute this representation error:

$$e_t^l = R_t(u) - \sum_{m \neq l} d_m \alpha_t(m). \tag{13}$$

– Set E_l as a matrix whose columns are $\{e_t^l\}_{t \in \omega_l}$.

– Apply SVD decomposition $E_l = U \Delta V^T$. Choose the updated dictionary columns d_l^{k+1} to be the first column of U. Update the coefficient values $\{\alpha_t^l\}_{t \in \omega_l}$ to be the entries of V multiplied by $\Delta(1,1)$.

3. Given all α_t, we can now fix those and turn to update u. Returning to Eq. (4), we need to solve

$$u^{k+1} = \arg\min_u \sum_{t=1}^{T} (\|D^{k+1}\alpha_t - R_t(u)\|_2^2) + \lambda_k \|u - v^{k+1}\|_2^2. \tag{14}$$

This is a simple quadratic term that has a closed-form solution of the form

$$u^{k+1} = \left(\lambda_k I + \sum_{t=1}^{T} R_t^T R_t\right)^{-1} \left(\lambda_k v^{k+1} + \sum_{t=1}^{T} R_t^T D^{k+1} \alpha_t\right). \tag{15}$$

4. Output: u^{k+1}, D^{k+1}.

where D^k is the dictionary obtained by the kth iteration, and σ_{k+1}^2 is the estimated variance from v^{k+1}.

C. Variance Estimation of Deblurred Image

Here, we propose to extend the idea of iterative regularization to update the noise variance σ_{k+1}^2 from v^{k+1}.

For the image v^{k+1} in Eq. (9), its noise contains two parts: One is the feedback of regularized noise from y, and the other one is the leaked noise in the denoised image $u^k = u_{\text{orig}} + \gamma^k$:

$$\mathcal{F}(v^{k+1}) = \mathcal{F}(u_{\text{orig}}^{k+1}) + \mathcal{F}(\gamma_{k+1,1}) + \mathcal{F}(\gamma_{k+1,2}), \tag{16}$$

where

$$u_{\text{orig}}^{k+1} = \mathcal{F}^{-1}\left(\frac{|\mathcal{F}(h)|^2 \cdot \mathcal{F}(u_{\text{orig}}) + r^k \mathcal{F}(u_{\text{orig}})}{|\mathcal{F}(h)|^2 + r^k}\right), \tag{17}$$

$$\gamma_{k+1,1} = \mathcal{F}^{-1}\left(\frac{\mathcal{F}(h)^* \cdot \mathcal{F}(\gamma)}{|\mathcal{F}(h)|^2 + r^k}\right), \tag{18}$$

$$\gamma_{k+1,2} = \mathcal{F}^{-1}\left(\frac{r^k \mathcal{F}(\gamma^k)}{|\mathcal{F}(h)|^2 + r^k}\right). \tag{19}$$

Then, the variance of $\gamma_{k+1,1}$ can be computed as

$$\begin{aligned} \sigma_{k+1,1}^2 &= E(|\langle \gamma_{k+1,1}, \gamma_{k+1,1} \rangle|^2) \\ &= \text{Var}(\gamma) \left\| \frac{\mathcal{F}(h)^*}{|\mathcal{F}(h)|^2 + r^k} \right\|^2 \\ &= \sigma^2 \left\| \frac{\mathcal{F}(h)^*}{|\mathcal{F}(h)|^2 + r^k} \right\|^2, \end{aligned} \tag{20}$$

where Var() is the variance.

Similar to $\gamma_{k+1,1}$, the variance of leaked noise $\gamma_{k+1,2}$ in the denoised image u^k can be estimated as

$$\sigma_{k+1,2}^2 = \text{Var}(\gamma^k) \left\| \frac{r^k}{|\mathcal{F}(h)|^2 + r^k} \right\|^2, \tag{21}$$

$$\text{Var}(\gamma^k) = c_0(\sigma_k^2 - \|v^k - u^k\|_2^2), \tag{22}$$

where σ_k^2 is the noise variance of v^k, $\|v^k - u^k\|_2^2$ means the variance of removed noise, and c_0 is a scaling factor controlling the re-estimation of noise variance.

Finally, we update the noise variance in the v^{k+1} as

$$\sigma_{k+1} = c_1 \sqrt{\sigma_{k+1,1}^1 + \sigma_{k+1,2}^2}, \tag{23}$$

where c_1 is also a scaling factor.

An intuitive explanation of Eq. (23) is as follows. As the iteration starts, only strong signals (with large coefficients) can contribute to the initial estimate of u; however, the partially recovered signal will be fed back to the noisy observation through Eq. (9), which helps lower the estimation of noise. In return, weaker signals can be identified and added to the signal estimate. As the iteration progresses, we usually observe that the estimated noise variance monotonically decreases; meanwhile, image structures are progressively recovered.

We summarize the main steps of the proposed image deconvolution algorithm as shown in Algorithm 2.

Algorithm 2: Image Deconvolution via Dictionary Learning

1. Initialization: $u^0 = 0$, $D^0 = \text{ODCT}$, $\sigma_0^2 = \sigma^2$

2. Iterate on $k = 0, 1, \ldots, iter$

– Iterative regularization: obtain v^{k+1} using Eq. (9).

– Noise variance update: reestimate noise variance σ_{k+1}^2 from v^{k+1} via Eq. (23).

– Image denoising via dictionary learning: update dictionary D^{k+1} and obtain an improved denoised image u^{k+1} using Eq. (15).

3. Output: u^{iter}.

Table 1. Comparison of the Output INSR (dB) of the Proposed Deblurring Algorithm[a]

Method	Exp 1	Exp 2	Exp 3	Exp 4	Exp 5	Exp 6	Exp 7	Exp 8	Exp 9
BNSR	29.16	40	15.99	26.61	40	16.47	40	17.35	28.07
Ours	**9.38**	**12.21**	**5.41**	**5.18**	**8.40**	**4.61**	**6.02**	**2.15**	**1.47**
ForWaRD	7.35	9.56	3.19	3.85	6.97	3.50	4.02	0.94	0.98
TVS	7.98	10.39	4.49	4.65	7.47	3.61	3.49	0.63	0.75
L0-AbS	8.40	11.06	4.55	4.80	7.79	4.22	3.98	0.73	0.81
SURE-LET	8.71	10.72	4.35	4.26	7.96	4.25	4.24	1.13	1.06
BM3DDEB	9.32	10.85	5.13	4.56	7.97	4.37	5.86	1.90	1.28
BSDL	9.32	6.99	5.22	4.88	4.83	4.50	2.65	2.00	1.13

[a]Blurred signal-to-noise ratio (BSNR) is defined as $\mathrm{BSNR} = 10\log_{10}\mathrm{Var}(y)/N^2\sigma^2$, where Var() is the variance.

4. Simulations

In all the simulations, the choice of β in Eq. (10) is taken as 1.5 as that is a good balance between efficiency and performance. The parameters c_0 in Eq. (21) and c_1 in Eq. (23) empirically are set as 0.4 and 1.25, respectively. The dictionaries used were of size 64×256, designed to handle image patches of size 8×8 pixels ($L = 64$, $K = 256$). In Algorithm 1, we choose $C_0 = 1.5$, and $\lambda_k = 30/\sigma_{k+1}$.

To evaluate our method for the nonblind deblurring task, we consider nine benchmark deblurring problems. In these simulations, original images are House of size 256×256 (experiments 1, 2, 3, and 4), Lena of size 512×512 (experiments 5 and 6), and Barbara of size 512×512 (experiments 7, 8, and 9). In our simulations, the blur PSFs we used are

- PSF1: $h_{ij} = (1 + i^2 + j^2), i, j = -7, \ldots, 7$
- PSF2: 9×9 *uniform*
- PSF3: $[1, 4, 6, 4, 1]^T[1, 4, 6, 4, 1]/256$
- PSF4: 25×25 Gaussian with std $= 1.6$

All PSFs are normalized so that $\sum h = 1$.

We summarizes different degradation models used, which are defined by the blur type and the variance of the AWGN for each of the experiments as follows:

- Experiment 1: PSF1, $\sigma^2 = 2$, and House
- Experiment 2: PSF2, $\sigma^2 = 0.165$, and House
- Experiment 3: PSF3, $\sigma^2 = 49$, and House
- Experiment 4: PSF4, $\sigma^2 = 4$, and House
- Experiment 5: PSF2, $\sigma^2 = 0.195$, and Lena
- Experiment 6: PSF4, $\sigma^2 = 4$, and Lena
- Experiment 7: PSF2, $\sigma^2 = 0.242$, and Barbara
- Experiment 8: PSF3, $\sigma^2 = 49$, and Barbara
- Experiment 9: PSF4, $\sigma^2 = 4$, and Barbara

They are used in other papers [13,18] and go from strong-blur/weak-noise to weak-blur/strong-noise cases.

Table 1 presents a comparison of the proposed algorithm versus a number of algorithms including the current state of the art. In this section, we present results of our proposed algorithm and compare it against competing deblurring methods such as ForWaRD [7], TVS [6], BM3DDEB [13], BLDL [16], L0-AbS [18], and SURE-LET [20]. We use the default parameters suggested by the authors for the competing algorithms.

In these experiments we will use the improvement in signal-to-noise-ratio (ISNR) to measure the performance. The ISNR is defined as

$$\mathrm{ISNR} = 10\log_{10}\left(\frac{\|u_{\mathrm{orig}} - y\|_2^2}{\|u_{\mathrm{orig}} - \hat{u}\|_2^2}\right), \tag{24}$$

where $\hat{u}$ is the corresponding estimated image.

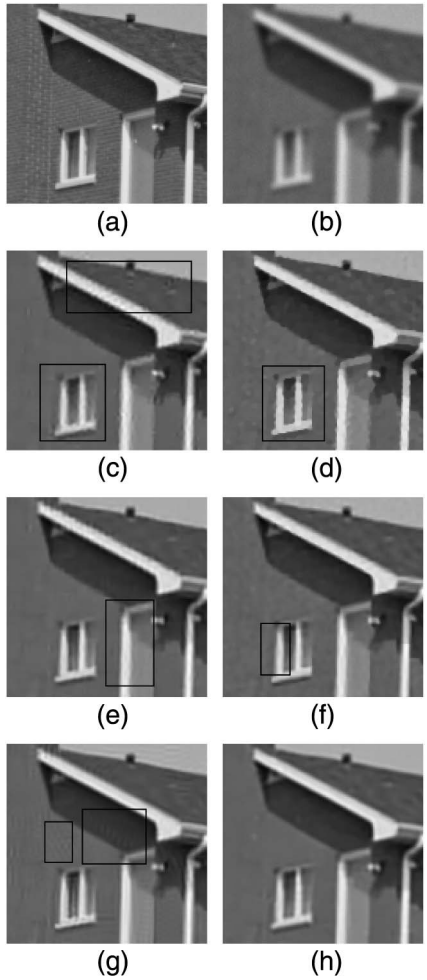

Fig. 1. Visual comparison of House image in experiment 4. (a) Original image; (b) blurred image; (c) ForWaRD result, ISNR = 3.85 dB; (d) TVS result, ISNR = 4.65 dB; (e) L0-AbS result, ISNR = 4.80 dB; (f) SURE-LET, ISNR = 4.26 dB; (g) BM3DDEB, ISNR = 4.56 dB; (h) our result, ISNR = 5.18 dB.

In the first set of experiments (1–4), a House image is blurred by four different PSFs. The ISNR values obtained by the different methods are compared in Table 1 under the Exp 1–4 columns. As can be seen from the ISNR, our algorithm shows the best performance compared to other image deconvolution methods. In Fig. 1, we show the details of the images obtained by the different methods in experiment 4. As can be seen from the Fig. 1(c), the result of ForWaRD [7] obtains a low contrast image with some visual artifacts. The result of TVS [6] is shown in Fig. 1(d)—there are some blocking artifacts in the image; and the L0-Abs [18] result is shown in Fig. 1(e), and it can be seen that the vertical white edge of the wall is still blurry. Figure 1(f) shows the result of SURE-LET [20]. By carefully examining it, there are a few artifacts around the vertical edges in the window. Figure 1(g) shows the result of BM3DDEB [13]; it obtains an image with obvious artifacts. Our result is shown in Fig. 1(h); one can see that our method recovers the sharpness of some edges (for instance, vertical edges in the window).

The second set of experiments (5 and 6) was performed on the Lena image. The simulation results are reported under the Exp 5–6 columns of Table 1, respectively. The proposed method yields ISNR values better than the values obtained by any of the other methods. The details of the images obtained by the different methods in experiment 5 are shown in Fig. 2. As can be seen from the figure, the slight difference among them in the visual performance is around the side of Lena's eyes.

In the third set of tests (Exp 7–9), a Barbara image is blurred by three different PSFs. The results are summarized under the Exp 7–9 columns of Table 1. From Table 1, we notice that our method performs the best in terms of ISNR. A portion of the deblurred images from different methods is shown in Fig. 3. The restoration result of ForWaRD [7] is shown in Fig. 3(c). By carefully examining it, there are some visually annoying artifacts in the image. The result of the TVS [6] obtains a blurred and noisy image, which is shown in Fig. 3(d). The results of L0-Abs [18] and SURE-LET [20] are shown in Fig. 3(e) and Fig. 3(f), respectively. It can be seen that the most details on

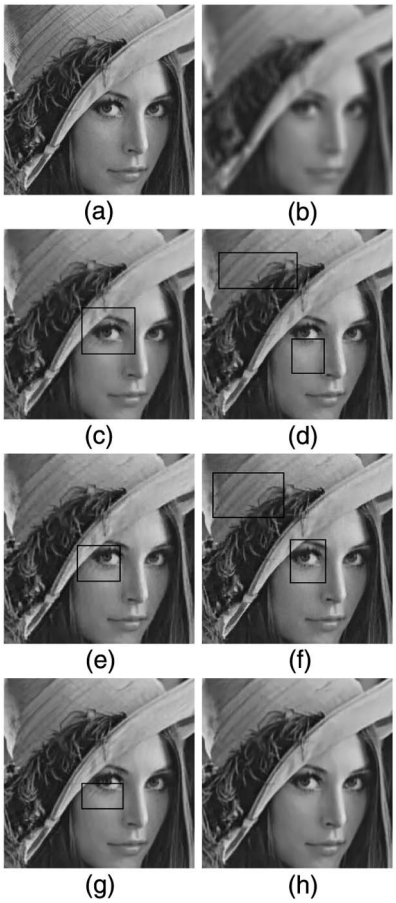

Fig. 2. Details of the image deconvolution experiment with Lena in experiment 5. (a) Crop from Lena image; (b) blurred image; (c) ForWaRD result, ISNR = 6.97 dB; (d) TVS result, ISNR = 7.47 dB; (e) L0-AbS result, ISNR = 7.79 dB; (f) SURE-LET result, ISNR = 7.96 dB; (g) BM3DDEB result, ISNR = 7.97 dB; (h) our result, ISNR = 8.40 dB.

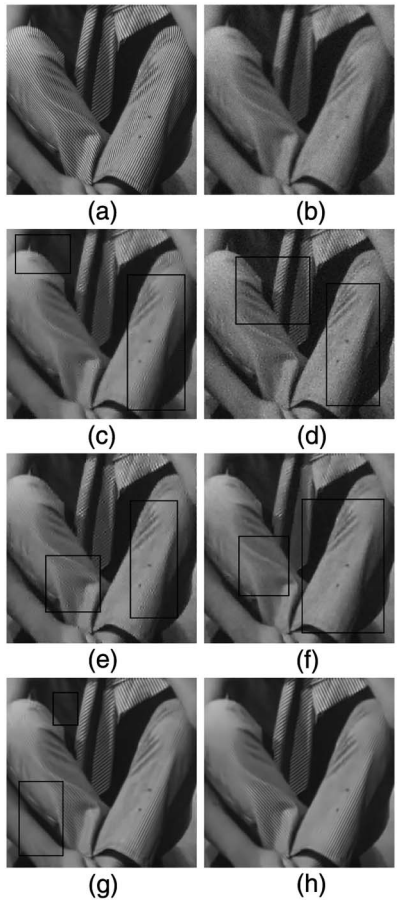

Fig. 3. Details of the image deconvolution experiment with Barbara in experiment 8. (a) Crop from Barbara image; (b) blurred image; (c) ForWaRD result, ISNR = 0.94 dB; (d) TVS result, ISNR = 0.63 dB; (e) L0-AbS result, ISNR = 0.73 dB; (f) SURE-LET result, ISNR = 1.13 dB; (g) BM3DDEB result, ISNR = 1.90 dB; (h) our result, ISNR = 2.15 dB.

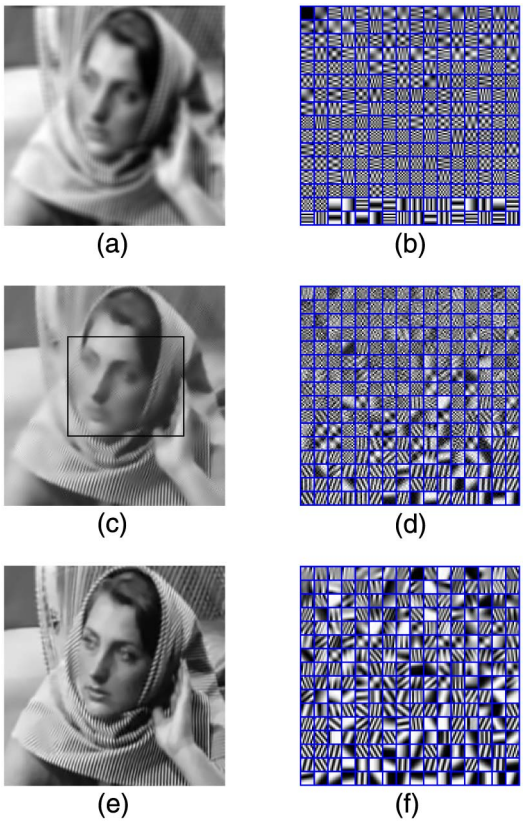

Fig. 4. Example of the deconvolution results of Barbara image in experiment 7. (a) Blurred image; (b) ODCT; (c) BSDl result, ISNR = 2.65; (d) learned dictionary of BSDL; (e) our deblurred result, ISNR = 6.02; (f) our final dictionary.

Barbara's trousers are lost. The restoration result of BM3DDEB [13] is shown in Fig. 3(g), there are a few artifacts around the side of trousers. The restoration result of our proposed method is shown in Fig. 3(h). One can see that it is more visually pleasant than Figs. 3(c)–3(g). Results have shown that the dictionary learning-based method obtains a deblurring result with better quantitative and visual performance.

Figure 4 describes the deconvolution process of experiment 7. Each iteration improves the deconvolution results, with the initial dictionary set to be the overcomplete discrete cosine transform (ODCT) [see Fig. 4(b)]. The restoration result of our proposed method is shown in Fig. 4(f), and the final adaptive dictionary that leads to the result is presented in Fig. 4(e). The results of BSDL [16] and the learned dictionary are shown in Fig. 4(c) and Fig. 4(d), respectively. It can be seen that Barbara's face is still blurry, and the dictionary is noisy.

5. Conclusion and Future Work

In this paper, we proposed a new formulation for image deconvolution using a dictionary learning strategy and a penalized splitting approach. A splitting method was presented to decouple the difference operators and dictionary. We also proposed a approach to update the estimation of noise variance for dictionary learning. The proposed method was tested using synthetic experiments and outperformed five existing state-of-the-art deconvolution algorithms. Future work will consist of extending the approach to the blind deblurring problem, where a blur kernel has to be learned at the same time as the learned dictionaries.

The authors would like to thank the support by the 2013 Jilin Province Post-doctor Research Program (RB20131).

References

1. A. K. Jain, "Image filtering and restoration," in *Fundamentals of Digital Image Processing* (Prentice-Hall, 1989), Chap. 7, pp. 267–341.
2. A. K. Katsaggelos, ed., "Introduction," in *Digital Image Restoration* (Springer-Verlag, 1991), Chap. 1, pp. 24–41.
3. P. C. Hansen, *Rank-Deficient and Discrete Ill-Posed Problems: Numerical Aspects of Linear Inversion* (SIAM, 1998).
4. Y. Wang, J. Yang, W. Yin, and Y. Zhang, "A new alternating minimization algorithm for total variation image reconstruction," SIAM J. Imag. Sci. **1**, 248–272 (2008).
5. J. Oliveira, J. M. Bioucas-Dias, and M. A. Figueiredo, "Adaptive total variation image deblurring: a majorization–minimization approach," Signal Process. **89**, 1683–1693 (2009).
6. O. V. Michailovich, "An iterative shrinkage approach to total-variation image restoration," IEEE Trans. Image Process. **20**, 1281–1299 (2011).
7. R. Neelamani, H. Choi, and R. G. Baraniuk, "ForWaRD: Fourier-wavelet regularized deconvolution for ill-conditioned systems," IEEE Trans. Signal Process. **52**, 418–433 (2004).
8. V. M. Patel, G. R. Easley, and D. M. Healy, Jr., "Shearlet-based deconvolution," IEEE Trans. Image Process. **18**, 2673–2685 (2009).
9. H. Yang and Z. Zhang, "Fusion of wave atom-based Wiener shrinkage filter and joint non-local means filter for texture-preserving image deconvolution," Opt. Eng. **51**, 67–75 (2012).
10. J. A. Guerrero-Colon, L. Mancera, and J. Portilla, "Image restoration using space-variant Gaussian scale mixtures in overcomplete pyramids," IEEE Trans. Image Process. **17**, 27–41 (2008).
11. A. Foi, K. Dabov, V. Katkovnik, and K. Egiazarian, "Shape-adaptive DCT for denoising and image reconstruction," Proc. SPIE **6064**, 203–214 (2006).
12. K. Dabov, A. Foi, V. Katkovnik, and K. Egiazarian, "Image denoising by sparse 3D transform-domain collaborative filtering," IEEE Trans. Image Process. **16**, 2080–2095 (2007).
13. K. Dabove, A. Foi, V. Katkovnik, and K. Egiazarian, "Image restoration by sparse 3D transform-domain collaborative filtering," Proc. SPIE **6812**, 681207 (2008).
14. H. Yang, M. Zhu, Z. Zhang, and H. Huang, "Guided filter based edge-preserving image non-blind deconvolution," in *Proceedings of the 20th IEEE International Conference on Image Processing (ICIP)*, Oral, Melbourne, Australia, September 2013.
15. H. Yang, Z. Zhang, M. Zhu, and H. Huang, "Edge-preserving image deconvolution with nonlocal domain transform," Opt. Laser Technol **54**, 128–136 (2013).
16. F. Couzinie, J. Mairal, F. Bach, and J. Ponce, "Dictionary learning for deblurring and digital zoom," Technical Report, HAL:inria-00627402, 2011.
17. L. Yuan, J. Sun, L. Quan, and H.-Y. Shum, "Progressive inter-scale and intra-scale non-blind image deconvolution," ACM Trans. Graph. **27**, 74 (2008).
18. J. Portilla, "Image restoration through l0 analysis-based sparse optimization in tight frames," in *Proceedings of the 16th IEEE International Conference on Image Processing (ICIP)*, Cairo, Egypt, 2009, pp. 3909–3912.
19. J. Ni, P. Turaga, V. M. Patel, and R. Chellappa, "Example-driven manifold priors for image deconvolution," IEEE Trans. Image Process. **20**, 3086–3096 (2011).
20. F. Xue, F. Luisier, and T. Blu, "Multi-Wiener SURE-LET deconvolution," IEEE Trans. Image Process. **22**, 1954–1968 (2013).

21. H. Yang, M. Zhu, H. Huang, and Z. Zhang, "Noise-aware image deconvolution with multi-directional filters," Appl. Opt. **52**, 6792–6798 (2013).
22. M. Elad and M. Aharon, "Image denoising via sparse and redundant representations over learned dictionaries," IEEE Trans. Image Process. **15**, 3736–3745 (2006).
23. Q. Liu, S. Wang, L. Ying, X. Peng, Y. Zhu, and D. Liang, "Adaptive dictionary learning in sparse gradient domain for image recovery," IEEE Trans. Image Process. **22**, 4652–4663 (2013).
24. J. Romberg, "Imaging via compressive sampling (introduction to compressive sampling and recovery via convex programming)," IEEE Signal Process. Mag. **25**(2), 14–20 (2008).
25. B. A. Olshausen, *Highly Overcomplete Sparse Coding: IS&T/SPIE Electronic Imaging* (SPIE, 2013).
26. B. A. Olshausen, "Emergence of simple-cell receptive field properties by learning a sparse code for natural images," Nature **381**, 607–609 (1996).
27. M. Elad, F. Mario, and Y. Ma, "On the role of sparse and redundant representations in image processing," Proc. IEEE **98**, 972–982 (2010).
28. E. Pennec and S. Mallat, "Sparse geometric image representations with bandelets," IEEE Trans. Image Process. **14**, 423–438 (2005).
29. M. Do and M. Vetterli, "Frame pyramids," IEEE Trans. Signal Process. **51**, 2329–2342 (2003).
30. E. Candes, L. Demanet, D. Donoho, and L. X. Ying, "Fast discrete curvelet transforms," Multiscale Model. Simul. **5**, 861–899 (2006).
31. S. Mallat, *A Wavelet Tour of Signal Processing* (Academic, 2008).
32. P. Chatterjee and P. Milanfar, "Clustering-based denoising with locally learned dictionaries," IEEE Trans. Image Process. **18**, 1438–1451 (2009).
33. J. Mairal, F. Bach, J. Ponce, G. Sapiro, and A. Zisserman, "Non-local sparse models for image restoration," in *Proceedings of the IEEE International Conference on Computer Vision*, Kyoto, Japan, September/October 2009, pp. 2272–2279.